JOURNAL OF MATERIALS SCIENCE 29 (1994) 4718–4728

Strength distribution of Carborundum polycrystalline SiC fibres as derived from the single-fibre–composite test

W. A. CURTIN*
BP Research/Carborundum Co., 4440 Warrensville Ctr. Road, Cleveland, OH 44128 USA
A. N. NETRAVALI, J. M. PARK
Department of Textiles and Apparel, Cornell University, Ithaca, NY 14853, USA

The single-fibre–composite (s.f.c) test, in which a fibre is embedded in an epoxy matrix and the composite tested in tension, was employed to obtain the statistical strength distribution of Carborundum SiC ceramic fibres over the range of gauge lengths from 0.5 to 20 mm. The raw s.f.c. test data was organized into three independent forms: the number of fibre breaks versus applied stress; the fibre fragment length distribution at the end of the test; and the fibre strength versus fragment length during testing. The data was interpreted using two different models of the fibre/epoxy–matrix interface, and it was found that a constant shear stress model could not self-consistently fit all of the s.f.c. data, whereas an elastic interface model provided good fits to all of the data. The applicability of the elastic interface model was supported by the absence of interfacial debonding and the rough fibre/matrix interface, which promoted mechanical interlocking. The s.f.c. test derived strength of $\sigma_0 = 1500$ MPa at a gauge length of 20 mm, with a Weibull modulus of $m = 9$, agreed fairly well with independent tension test results obtained on 254 mm length samples. Obtaining self-consistent fits to all of the manifestations of the s.f.c. data requires careful testing and analysis, but the present work demonstrates that the s.f.c. test can be a powerful tool for the accurate and independent assessment of fibre strengths at small gauge lengths.

1. Introduction

The dependence of average brittle fibre strength on tested gauge length is well documented [1]. Since the fibre strength is determined by its weakest flaw, the typical fibre strength increases as the length tested decreases. Such a gauge length dependence (size effect) of fibre strength is important in composite applications because the mechanics within the composite establish a gauge length, l_c, often called the critical [2] or ineffective [3] length, and the composite strength is then controlled by the fibre strength at the length l_c. Unfortunately, l_c is typically of the order of millimetres or smaller and tension testing of single fibres at such gauge lengths can be rather difficult to perform reliably. A technique which avoids such difficulties is the single-fibre composite (s.f.c.) test [2, 4–9]. In the s.f.c. test a single fibre is embedded in a large failure strain epoxy and this "composite" is subjected to uniaxial tension. Under increasing load, the fibre undergoes successive fragmentation at its weakest points. Multiple breaks in the fibre can occur because the matrix holds the fibre along its length and transfers the applied load back into the fragments via shear across the fibre/matrix interface. As more breaks occur in the fibre the fibre fragments obviously decrease in size and, hence, information on the fibre strength at various lengths is contained in the number and location of breaks versus stress as recorded during the test. The fragmentation process ultimately ceases when the fragments are small enough that the tensile stress in the fibre, which is zero at each break point, cannot build up to the applied value, i.e. when the fragments are roughly twice the load transfer, or ineffective, length governing transfer of load from the matrix to the fibre. For typical combinations of fibre and epoxy the final fragment sizes are of the order of 1 mm and so the s.f.c. fragmentation data contains information on the dependence of strength versus fibre gauge length down to the gauge lengths of interest in composite applications.

In this work, the s.f.c. test was used to derive the statistical strength distribution of sintered polycrystalline SiC fibres obtained from the Carborundum Co. over the range of gauge lengths from 0.5 to 20 mm. Interpretation of the s.f.c. data requires a knowledge of the fibre/matrix interfacial properties. Because of the

* *Present address*: Departments of Material Science and Engineering and Engineering Science and Mechanics, Virginia Polytechnic Institute State University, Blacksburg, VA 24060, USA.

0022–2461

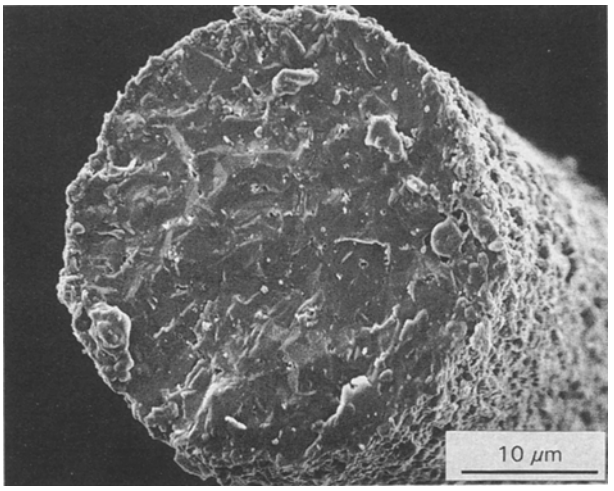

Figure 1 Micrograph of a polycrystalline SiC fibre used in this work; note the rough surface.

roughness of the polycrystalline SiC fibres investigated here (Fig. 1), it is argued that mechanical bonding and/or interlocking between the fibre and the matrix inhibits decohesion of the fibre/matrix interface and, hence, that a well-bonded elastic interface model is appropriate for this system. Such a model is in distinct contrast to most other fibre/matrix systems, where interfacial debonding and/or matrix yielding do occur during the s.f.c. test [4–9]. Assuming an elastic interface model, all of the experimental data was compared to new theoretical results obtained by computer simulations. A fibre scale strength of 1500 MPa at a 20 mm gauge length, with a Weibull modulus of m = 9, was found to agree well with all aspects of the observed fragmentation data over the range of 0.5–20 mm. In contrast, self-consistent fits to the experimental data, assuming a constant interfacial shear stress model, could not be found. The scale strength and Weibull modulus derived here are in general agreement with single fibre tension test results obtained at larger gauge lengths.

The remainder of this paper is organized as follows. In the next section, the background mechanics used to describe the fibre/matrix interfacial behaviour and also formalize the concept of a statistical strength distribution for brittle fibres is discussed. In Section 3, the details of s.f.c. sample preparation, experimental procedures and data are discussed. In Section 4, the general theoretical results for both constant shear stress and elastic shear stress interfaces are presented, comparisons are made with the experimental data obtained and the fibre strength statistics deduced. Section 5 contains further discussion of the findings and their implications on the performance of ceramic composites utilizing this fibre.

2. Interfacial mechanics and fibre strength statistics

2.1. Interfacial mechanics

A full interpretation of the s.f.c. test data requires knowledge of the detailed mechanics at the fibre/matrix interface. Starting from zero at a break, the axial tensile stress in the fibre builds up by load transfer via the shear stress across the fibre/matrix interface. Denoting the shear stress a distance x from the fibre break location by $\tau(x)$, then the (average) axial fibre stress is

$$\sigma(x) = \frac{4}{d}\int_0^x dx'\tau(x') \quad (1)$$

where d is the fibre diameter. In general, the axial stress, σ, near any existing break is lower than the value at points far from the break, and hence the probability of finding further breaks near an existing break is lower than that for breaks remote from the existing breaks. Fibre breaks in the s.f.c. test tend, therefore, to be spaced by at least some length determined by the shear stress $\tau(x)$. The mixing of the fibre strength distribution with a spatially varying axial stress as breaking progresses makes the prediction of the break evolution a difficult problem. Conversely, with the s.f.c. test data in hand, the inversion of the data to derive both the fibre strength distribution and the interfacial shear stress $\tau(x)$ can be formidable.

To simplify the general problem, some basic physics and mechanics considerations motivate a flexible but tractable class of functions for the shear stress $\tau(x)$. Specifically, under conditions of perfect elastic bonding between a cylindrical fibre and the matrix, Cox [10] used a shear lag approach to obtain the stresses

$$\tau(x) = \alpha\sigma_{app}e^{-\beta x} \quad (2a)$$

$$\sigma(x) = \sigma_{app}(1 - e^{-\beta x}) \quad (2b)$$

for a semi-infinite fibre under a remote tensile stress,

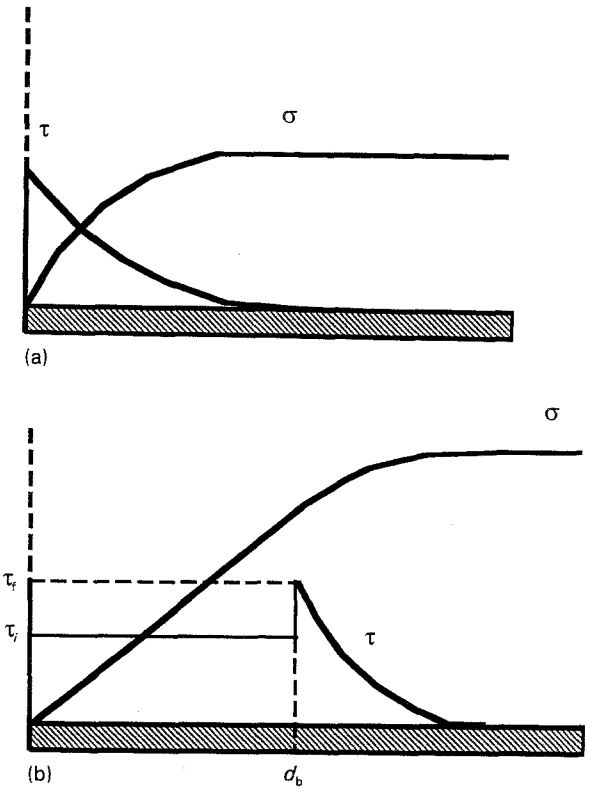

Figure 2 (a) Axial and shear stresses versus distance from fibre break from shear lag model of an elastic interface. (b) As (a), but for a debonded interface.

σ_{app}, as shown in Fig. 2a. Here,

$$\alpha = (G_m/2KE_f)^{1/2}; \beta = 4\alpha/d \quad (2c)$$

where G_m is the matrix shear modulus, E_f the fibre Young's modulus and K a geometrical constant of order unity. If the fibre/matrix interface can only sustain a maximum shear stress τ_f (which could correspond to the shear yield stress of the matrix or the adhesive shear strength of the interface), then Equation 2 ceases to be valid for $\sigma_{app} > \tau_f\alpha$. For loads beyond interfacial failure, a debonded or yielded region can form which is modelled by a region of constant shear stress τ_i. τ_i may correspond to the matrix yield stress itself or to a frictional shear stress behind an advancing debond at the interface. The general situation is shown in Fig. 2b, and is described mathematically by

$$\tau(x) = \tau_i \quad x \leqslant d_b \quad (3a)$$
$$= \tau_f e^{-\beta(x-d_b)} \quad x > d_b$$

and

$$\sigma(x) = 4\tau_i x/d \quad x \leqslant d_b$$
$$= 4\tau_i d_b/d + \frac{\tau_f}{\alpha}(1 - e^{-\beta(x-d_b)}) \; x > d_b \quad (3b)$$

d_b is the length of the debond and is related to the applied tensile stress, σ_{app}, by

$$d_b = \frac{d}{4\tau_i}[\sigma_{app} - \tau_f/\alpha] \quad \sigma_{app} \geqslant \tau_f/\alpha \quad (4)$$

Equations 2–4 capture a broad range of interfacial behaviours in terms of only two parameters, τ_f and τ_i (the parameters β and α are not dependent on interfacial properties but only on bulk material properties).

For finite fibre fragment lengths, the stress recovery from the two ends will overlap and modify Equations 2–4. For the case of perfect elastic bonding behaviour, corresponding to $\tau_f = \infty$ (see Fig. 2a), the major effect on the axial stress is that the maximum axial stress along fragment of length l is [10]:

$$\sigma_{max} = \sigma_{app}\left[1 - \frac{1}{\cosh(\beta l/2)}\right] \quad (5a)$$

which occurs at the midpoint of the fragment. For constant τ_i and $\tau_f = 0$ the maximum stress is

$$\sigma_{max} = \sigma_{app} \quad > d\sigma_{app}/2\tau_i$$
$$= 2\tau_i/d \quad < d\sigma_{app}/2\tau_i \quad (5b)$$

In the subsequent discussion, two limiting cases of the above general interfacial model will be focussed upon. The first case is when $\tau_f \sim 0$ (specifically $\tau_f/\alpha \ll$ typical fibre strengths); this corresponds to very poor adhesion, such that the interfacial mechanics is dominated by the constant shear stress τ_i. The complete evolution of the fibre fragmentation in this case can be calculated exactly for any fibre strength statistics [11]. The second special case is large $\tau_f(\tau_f/\alpha \gg$ typical fibre strengths); this corresponds to very good adhesion. The evolution of fibre fragmentation in this case is not known exactly, and will be studied here by computer simulation.

2.2. Fibre strength distributions

A fibre contains a variety of flaws which will fail under a range of applied tensile stresses, and it is generally assumed that such flaws occur randomly along the length of the fibre. The quantity at the heart of the statistical description of brittle fibre strength is then the number of defects in a length L which are weaker than stress σ, which is denoted $\Phi(\sigma, L)$. Brittle materials are usually characterized empirically by a Weibull form [12] for the fibre defect distribution,

$$\Phi(\sigma, L) = \frac{L}{L_o}(\sigma/\sigma_o)^m \quad (6)$$

where m is the Weibull modulus describing the variability in fibre strength at any fixed length. The Weibull form in the present work is used as a flexible class of functions for describing fibre statistical strength. From Equation 6 it is clear that the scale stress, σ_0, is the stress at which there is typically one defect in a length L_0 of fibre, i.e. $\Phi(\sigma_0, L_0) = 1$. The probability of failure P_f versus stress for a fibre of length L, which would be determined by a number of single fibre tension tests, is obtained from $\Phi(\sigma, L)$ by a weakest-link argument as

$$P_f(\sigma, L) = 1 - \exp[-(L/L_0)(\sigma/\sigma_0)^m] \quad (7)$$

The probability of failure in a length L_0 at stress σ_0 is thus $P_f = 1 - e^{-1} = 0.632\ldots$, and the median (50% probability) failure stress is $\bar{\sigma} = (\ln 2)^{1/m}\sigma_0$.

Equation 6 implies a relationship between the typical strengths of fibres of different gauge lengths. Specifically, the scale stress, σ_L (63.2% probability), for fibres tested at gauge length L is related to the scale stress σ_0 at length L_0 by

$$\frac{\sigma_L}{\sigma_0} = \left[\frac{L_0}{L}\right]^{1/m} \quad (8)$$

Thus, given information on the fibre strength distribution at length L_0, in the form of σ_0 and m, the fibre strength distribution at any other length L is characterized by the same m and a scale strength σ_L. In practice, the parameters σ_0 and m determined at gauge length L_0 may not be relevant to the strength distribution at lengths $L \ll L_0$ or $L \gg L_0$ because the nature of the flaws establishing the distribution at length L_0 may be different from those at much different length scales. Since the gauge length l_c relevant in composites is often $l_c \ll L_0$, it is valuable to derive the scale strength and Weibull modulus for lengths on the order of l_c. The s.f.c. test offers this possibility, as noted earlier, and is used here to derive the strength and Weibull modulus of Carborundum SiC fibres at short gauge lengths.

3. Experimental details and results

3.1. Epoxy characterization and specimen preparation

The tensile properties of the bulk epoxy material were obtained by testing dog-bone shaped specimens. To fabricate specimens DER 331, biphenol-A based (DGEBA), liquid epoxy resin was cured using DEH No. 26, tetraethylenepentamine (TEPA), in stoichio-

metric proportion. This resin/curing agent combination was chosen to ensure that no matrix cracking occurred at the fibre fracture locations [8]. The resin and the curing agent were obtained from Dow Chemical Corporation. The resin and curing agent were thoroughly mixed, degassed in a vacuum chamber to remove air, and poured slowly into the dog-bone shaped silicone rubber mould. The mould containing the resin mixture was then put in an oven for curing. After curing for 3 h at 80 °C, the oven was turned off and the specimen allowed to cool slowly to room temperature. After taking the specimen out of the mould, it was polished using standard metallographic techniques to obtain smooth surfaces. The bulk epoxy specimens were tension tested using an Instron tension testing machine (Model 1122) at the strain rate of 0.005 min^{-1} and under standard conditions of 20 °C and 65% relative humidity. A set of three specimens were tested. From the Instron plot of load versus elongation, and the measured specimen thickness and width, the stress at any strain level could be calculated.

Another set of three specimens were heated to 80 °C. Their lengths were measured accurately, before and after heating, using a micrometre. The average thermal expansion coefficient of the cured epoxy was calculated from the length measurements at room temperature and 80 °C.

The s.f.c. specimens were fabricated as described above with the exception that the degassed mixture was cast into a mould containing a single SiC fibre (35 μm nominal diameter) suspended at half-depth along the centreline. Care was taken not to disturb the fibre or add any air bubbles during the pouring. After curing and polishing the specimens were transparent and suitable for optical microscopy.

3.2. Fibre fragmentation

A small strain frame that could be easily mounted on an Olympus model PME optical microscope was used to strain the s.f.c. specimen [8]. A dial gauge attached to the strain frame was used to measure the specimen strain. A torque meter was also attached to the strain frame to check the consistency of the starting/zero strain point. This was done because of the possibility of some specimens being mounted with a small amount of slack or compression. The Olympus microscope had the capability of observing the specimen under cross-polarizers so that birefringence patterns around the fibre breaks could be observed to assess the extent of debonding along the fibre and/or matrix cracking. No debonding or matrix cracking was observed during the tests; a typical micrograph of the birefringence patterns around a fibre break is shown in Fig. 3. The s.f.c. tests were conducted within three days after making the specimens to avoid any effects due to physical ageing.

To run a s.f.c. test, the specimen was strained in small increments of approximately 0.005 mm. After each strain increment, the test gauge length of the specimen (18–20 mm) was scanned optically to observe any fibre breaks. For every fibre break observed,

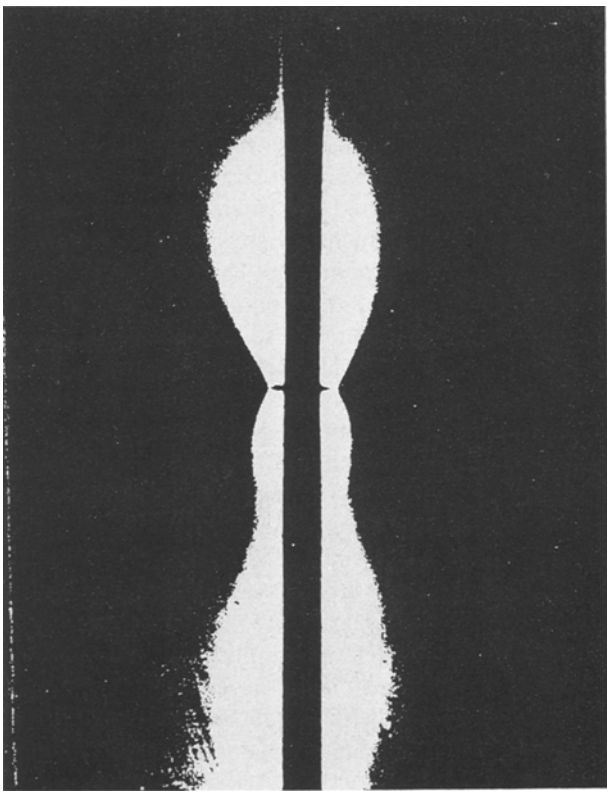

Figure 3 Birefringence pattern at a fibre break; the nodes at the break indicate that there is no debonding.

the location of the break and the strain on the specimen, obtained from the dial gauge, were noted. In a few cases, more than one additional break was found after a strain increment but such breaks were always widely separated, often on different fibre fragments. Each specimen was strained until no more breaks occurred for at least 2% additional strain. At this point, saturation was deemed to be achieved and all the fragment lengths within the gauge length were measured using a calibrated eyepiece. Measurements were also made of the fibre diameter at several different locations within the gauge length. A total of six s.f.c. specimens were studied in this manner, each test requiring several hours to complete.

The raw data from the s.f.c. test consisted of all the break locations and the corresponding specimen strains. The applied specimen stress, σ_{app}, at each fibre break was then calculated from the specimen strain using the load-elongation curve for the bulk epoxy specimens. Having obtained the stress in the epoxy, the stress σ_f in the fibre was then calculated as

$$\sigma_f = \frac{E_f}{E_m} \sigma_{app} - E_f \varepsilon_{thermal}$$

where $\varepsilon_{thermal}$ is the measured thermal strain of 0.25% due to the epoxy shrinkage on cooling which puts the fibre in a state of residual compression; E_f and E_m are the fibre and matrix moduli, respectively. E_f for the present fibres was 400 GPa. The fibre diameters used in the present tests varied between 34–36 μm but each individual fibre had a uniform diameter over the tested 20 mm gauge length.

3.3. Results

The number of breaks versus applied fibre stress σ_f for the six s.f.c. samples tested is shown in Fig. 4. On average, 36 breaks were obtained in the 20 mm gauge length, and the breaks occurred over a range of 1300–5600 MPa in applied stress. The sample-to-sample variations were fairly small, with the exception of one sample in which the stresses were uniformly a few hundred MPa higher. This one sample was fabricated and tested in a manner identical to the other five tests, however, and so there were no identifiable reasons for considering it to be particularly anomalous.

The distribution of fibre fragment lengths at the end of the s.f.c. test is shown in Fig. 5, where the lengths have been normalized to the mean fragment length for each test. The variations in fragment length run typically from 0.5 to 1.5 times the mean length, with an occasional smaller or larger fragment. The mean fragment lengths were typically 0.55 mm.

Fig. 6 shows the relationship between the breaking stresses at each break and the corresponding fragment length within which each break occurred. This strength versus "instantaneous gauge length" plot

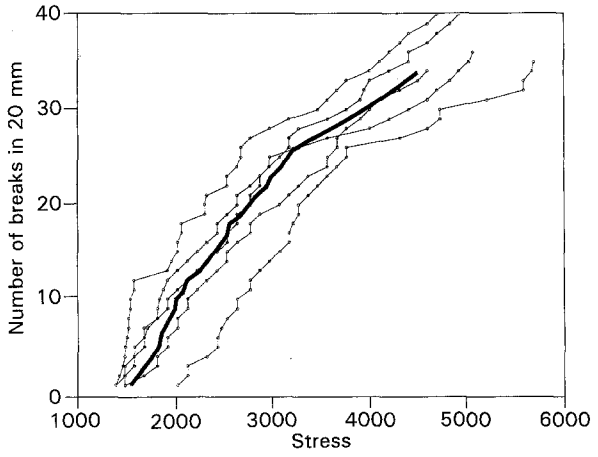

Figure 4 Number of breaks versus applied fibre stress for six different s.f.c. samples and average values.

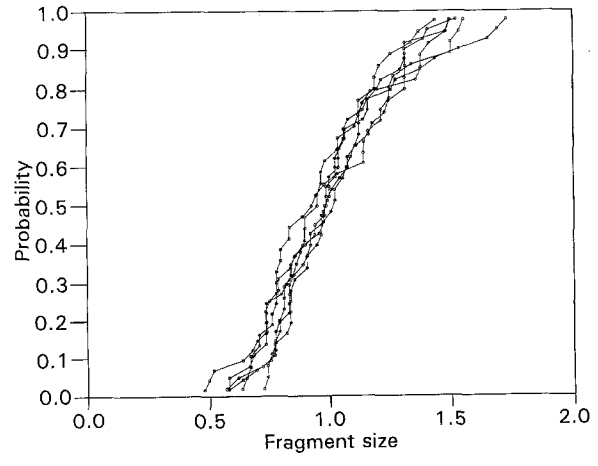

Figure 5 Cumulative fibre fragment distribution at the end of the s.f.c. tests; fragment lengths are normalized to the mean length.

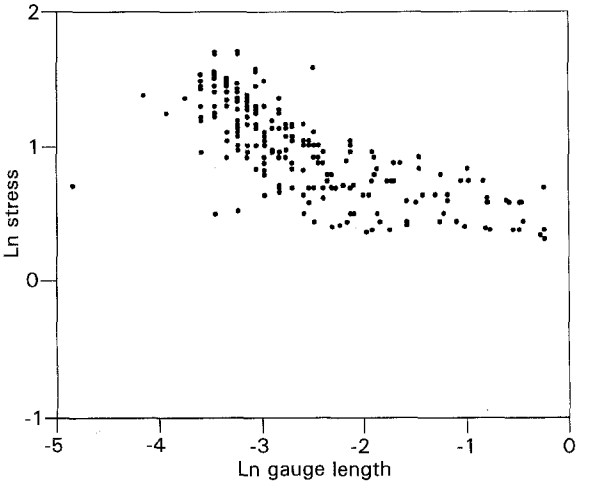

Figure 6 Fibre strength versus fragment size (or "instantaneous gauge length") for all s.f.c. samples, in InIn form.

gives some indication of the scaling of strength with fibre length, but is not precisely equivalent. In particular, the sharp rise in strength versus gauge length at small lengths is not a true reflection of the underlying fibre strength versus gauge length. As the fragments become smaller, the lower-stress recovery zones near each break occupies an increasing fraction of the fragment lengths and thus the true gauge length sampled is smaller than the fragment length. Furthermore, each fragment has, by definition, survived to a certain stress level during the test and is thus proof-tested prior to the occurrence of a break within the fragment. These two aspects make the strength versus instantaneous gauge length data a manifestation of the statistical fibre strength distribution and interfacial behaviour which is independent of the number of breaks versus stress (Fig. 4) and the final fragment distribution (Fig. 5).

In the following Section, our analysis of the data in Figs 4–6 is discussed to derive a set of fibre strength and interfacial shear parameters which account for these experimental results.

4. Theoretical results and data analysis

In this section the theoretical predictions for fragmentation under the two cases of constant shear stress, τ_i (poor adhesion), and elastic shear stress (good adhesion) are discussed. These theories are then used to fit the data obtained in Section 3, thereby deriving the appropriate scale strength and Weibull modulus for these SiC fibres.

4.1. Constant shear stress

When $\tau_f = 0$ and τ_i is constant, the axial fibre stress is linear from zero up to the applied load (Fig. 2a). The recovery length, δ, or slip length, is derived from Equation 1 by setting $\sigma(\delta) = \sigma_{app}$, which gives

$$\delta = \frac{d\sigma_{app}}{4\tau_i} \tag{9}$$

Because the stress within the recovery length does not

depend on the applied stress, it turns out that no further breaks can occur within the length $\pm \delta$ of any existing break. Consequently, the break evolution can be determined exactly [11]. The key result is that there is a characteristic fragment length, δ_R, which is the slip length at a characteristic stress, σ_R [11, 13]

$$\delta_R = \frac{d\sigma_R}{4\tau_i} \tag{10}$$

with the stress σ_R being the typical fibre strength at the gauge length $2\delta_R$, i.e.

$$\Phi(\sigma_R, 2\delta_R) = \frac{2\delta_R}{L_0}(\sigma_R/\sigma_0) = 1 \tag{11}$$

Equations 10 and 11 can be solved for δ_R and σ_R in terms of the material parameters σ_0, L_0, m, d and τ_i, and the fragmentation data is dependent only on δ_R and σ_R. For instance, the average fragment size $\langle l \rangle$ at the end of the test is $\langle l \rangle = \lambda(m)\delta_R$ where the dimensionless coefficient $\lambda(m)$ is known [11]. The fragment length distribution, with length normalized by $\langle l \rangle$, is also only dependent on m and not on the characteristic fibre strength, σ_R. Similarly, the cumulative fraction of breaks versus normalized stress σ/σ_R is only dependent on m and not on the characteristic length δ_R. Finally, in this case, there exists a well-defined "saturation" point beyond which no further breaks can occur because the fibre fragments are small enough that all points in the fragments were within the slip length, or recovery zone, of the fibre breaks and so can not be loaded any further, as evident from Equation 5b.

4.2. Elastic shear stress

When $\tau_i = 0$ and τ_f is large, the axial fibre stress in a fragment of length l is [10, 14]

$$\sigma(x) = \sigma_{app}\left[1 - \frac{\cosh(\beta l/2 - \beta x)}{\cosh(\beta l/2)}\right] 0 \leqslant x \leqslant l \tag{12}$$

Although there is a recovery zone of approximately $\pm \beta^{-1}$ in length, the stress everywhere in the fragment is proportional to the applied stress, σ_{app}. This allows for the possibility of subsequent fibre breaks within $\pm \beta^{-1}$ of existing breaks upon increased applied stress. Predicting the fragmentation under elastic shear stress cannot, to our knowledge, be done exactly because of this complication. This complication also implies that there is no well-defined "saturation" point during the s.f.c. test: the load σ_{app} can always be increased enough so that ever-stronger flaws in the fibre can be induced to break. The existence of a saturation point as found in the present experiments indicates that τ_f is large but finite. As physically expected, debonding/decohesion or yielding must occur at some stress level near the end of the test to give saturation behaviour. However, since most of the breaks occurred prior to such debonding or yielding, the only measurable evidence is a cessation of fibre breaking during the test.

To model fibre fragmentation under elastic shear stresses, numerical simulations must be used. The simulations are easy to perform and the procedure is as follows. A fibre of length L_0 is divided into M segments each of length $L_M \ll L_0$ (typically $M = 10^4$, $L_M = 10^{-4}L_0$), and each segment is randomly assigned a strength according to the Weibull cumulative probability distribution

$$P(\sigma, L_M) = 1 - e^{(-\sigma/\sigma_{L_M})^m} \tag{13}$$

where $\sigma_{LM} = \sigma_0 M^{1/m}$ is the fibre scale strength at the gauge length L_0/M. A uniform stress σ_f is gradually applied along the entire fibre length and a "break" is formed at a segment when the stress $\sigma(x)$ on the segment equals the assigned strength of that segment. The stress in each segment of any fragment, a fragment being bounded on either side by a break or the sample edge, is calculated via Equation 12. As the applied stress is increased, the applied stress at which each break occurred, the actual stress on the break and the break location are recorded and can later be converted into any form of data desired (e.g. number of breaks versus applied stress, fragment length distribution etc.). Algorithms to optimize the searching procedure were used to speed up the calculations, but the details are unimportant for the present discussion. The simulations require three independent parameters as input: the fibre statistical strength parameters σ_0 and m, and the elastic parameter β (which could be estimated by Equation 2c). The results are independent of M for large M, of course. For fixed values of σ_0 and m, the simulation generates a flaw distribution in the segments according to Equation 13 and each realization of the flaw distribution gives a particular fragmentation evolution. The average of six realization at each set of (σ_0, m, β) values are shown, since there are six experimental realizations for comparison; this will provide some estimate of whether the sample-to-sample statistical variations obtained experimentally are simply due to different statistical realizations at fixed (σ_0, m, β) or possibly other statistical or experimental uncertainties, such as errors in the residual stress corrections. Finally, for comparison with the experimental data, which does show a saturation in fibre breaking, the simulated tests must be cut off at some point to reflect the onset of debonding or yielding which must occur in the experiments. The cut-off imposed is a maximum applied axial fibre stress of 5 GPa, beyond which almost no breaks occur in the fibres tested here.

4.3. Data analysis

For both constant shear and elastic interface cases there are three independent parameters. The fibre scale strength σ_0 (at some length L_0) and Weibull modulus m are common parameters to both models. The scale strength σ_0 at $L_0 = 20$ mm (the s.f.c. sample gauge length) will be fitted in the following discussion, with the reminder that the best-fit values of σ_0 are obtained by fitting to s.f.c. data obtained from 0.5 to 20 mm; thus, the strength at all lengths between 0.5 and 20 mm can be derived from the strength σ_0 at 20 mm and the Weibull modulus m simply by using Equation 8. For the constant shear stress case the

third parameter is τ_i, while for the elastic interface case the third parameter is β (which is, however, estimated by Equation 2c). In this analysis, for each pair of fibre strength parameter values (σ_0, m), the value of τ_i or β is adjusted so that the average total number of breaks in a 20 mm sample is the measured value of 36 (plus or minus one break in the elastic shear stress case, since these results are numerically simulated). With this constraint, the two remaining adjustable parameters σ_0 and m are precisely those of primary interest in this work.

4.3.1. Constant shear stress

Predictions for the number of breaks versus stress and the final fragment distribution for the constant τ_i model as a function of σ_0 and m are compared with the average experimental results in Fig. 7a and b. Although the lower tail in N versus σ fitted fairly well with (σ_0 = 1500 MPa, m = 9) and (σ_0 = 1400 MPa, m = 6), the overall curve is more consistent with a much lower strength and much lower m, as evidenced by the results for (σ_0 = 1000 MPa, m = 3). However, for these lower values the fit in the low tail is not particularly good. A low Weibull modulus is required to account for the broad range of stresses over which breaks occur. On the other hand, the final fragment distribution is much more consistent with larger Weibull moduli m $\geqslant$ 6, as seen in Fig. 7b; small Weibull moduli give too large a spread in fragment sizes. The data on strength versus fragment length (Fig. 6) can not be directly obtained for this case, but just as the low tail of N versus σ is not at all consistent with small m and low σ_0, the data in Fig. 6 are incompatible with values in the range of (σ_0 = 1000 MPa, m = 3). It has been shown previously [15] that for large fragments $\geqslant L_0/10$, the

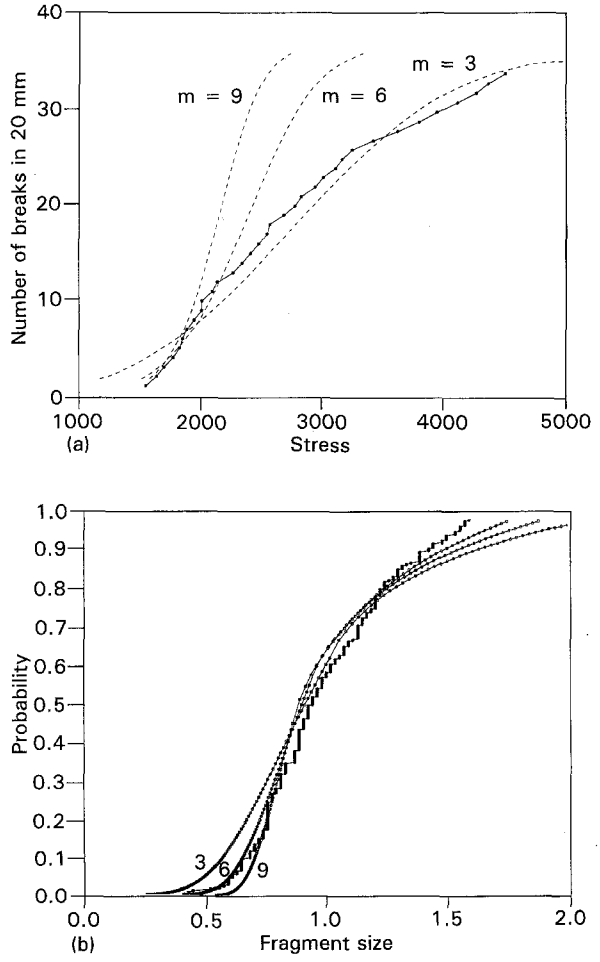

Figure 7 (a) Predicted number of breaks versus applied fibre stress for constant τ interface model for various (σ_0, m); also shown is average of data from Fig. 4. (b) Predicted cumulative fragment length distribution for constant τ interface model, for m = 3, 6, and 9; also shown is cumulant of all data from Fig. 5.

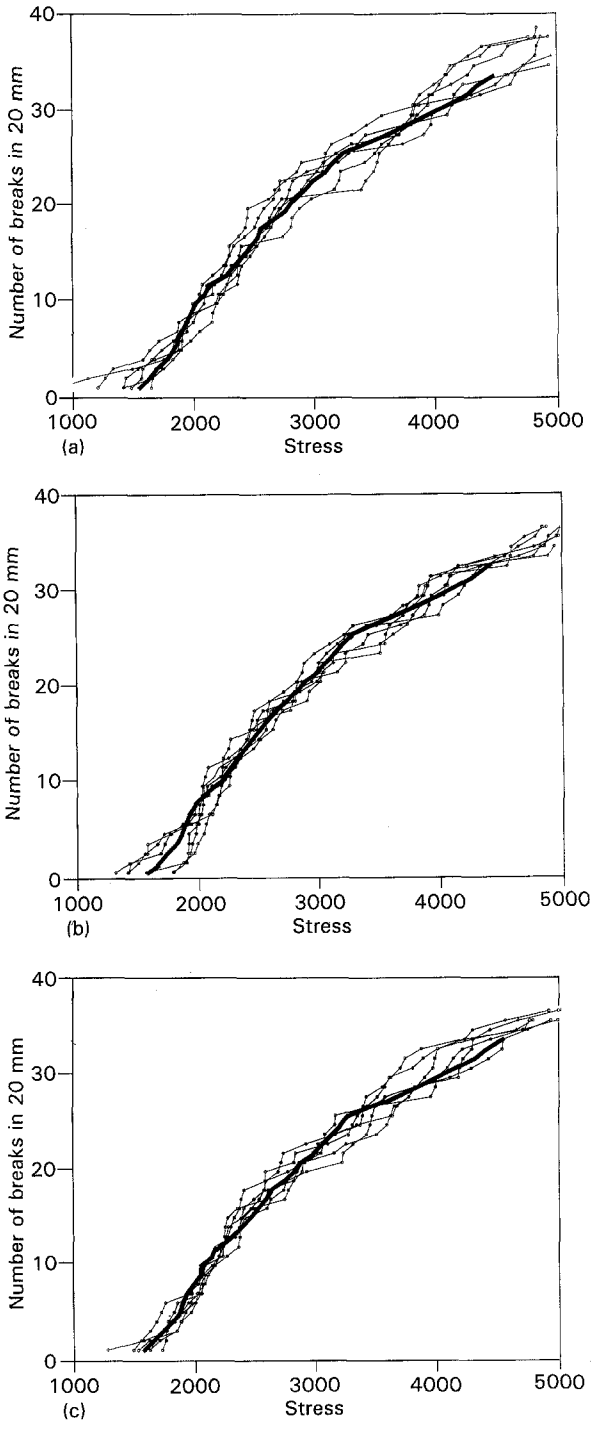

Figure 8 Predicted number of breaks versus stress for elastic shear stress interface model for various (σ_0, m, β^{-1}) values; also shown is average data from Fig. 4. (a) (σ_0 = 1400 MPa, m = 7, β^{-1} = 0.300 mm); (b) (σ_0 = 1500 MPa, m = 9, β^{-1} = 0.325 mm); (c) (σ_0 = 1600 MPa, m = 11, β^{-1} = 0.325 mm).

slope $-1/m^*$ of strength versus fragment length corresponds to an apparent Weibull modulus m^* which is related to the true m by $m \sim 1.5\, m^*$. In Fig. 6, $m^* \sim 6$ implying $m \sim 9$. Finally, for all values of σ_0, m shown in Fig. 7a, the corresponding values of τ_i ranged from 56 to 100 MPa. Since $\tau_i \leqslant \tau_f$ is expected physically, the condition $\tau_f/\alpha \ll \sigma_R$ required for the use of the constant shear stress approximation is not satisfied. Specifically, $\tau_f/\alpha > \tau_i/\alpha \sim 2000$–$2500$ MPa, whereas the typical derived fibre strength is $\sigma_R \sim 2200$–3200 MPa. Overall, it can be concluded that all of the present data cannot be adequately fit by any one pair of (σ_0, m) values under the assumption of a constant interfacial shear stress.

4.3.2. Elastic shear stress

The simulation results for the number of breaks versus stress for various (σ_0, m) values are compared to the average experimental results shown in Fig. 8a–c. Very close agreement is obtained for the parameter values ($\sigma_0 = 1400$ MPa, $m = 7$, $\beta^{-1} = 0.300$ mm), ($\sigma_0 = 1500$ MPa, $m = 9$, $\beta^{-1} = 0.325$ mm) and ($\sigma_0 = 1600$ MPa, $m = 11$, $\beta^{-1} = 0.325$ mm). Changes of only $\pm$ 100 MPa in the value of σ_0 at fixed m provide much less satisfactory fits. The results for the lower Weibull value of $m = 7$ do not fit the lower tail quite as well as the higher m values, but overall there is a general trade-off, over a narrow range, between increasing the fibre strength, σ_0, and increasing the Weibull modulus, m. The broad spread of applied stresses needed to break the fibres occur in spite of the high Weibull moduli for the elastic shear stress case, because of the suppression of the axial tensile fibre stress (due to overlap of the recovery zones from each end of the fibre) as expressed by Equation 5a. As the fragments become smaller the actual peak stress on the fragments could be rather lower than the applied stress; therefore, stresses much larger than the actual defect strengths must be applied to attain the stress levels needed in the fibre to break the fragments. As an example, Fig. 9 shows the actual strengths of flaws along one fibre along with the applied stresses necessary to fail those flaws (as in Fig. 7a) for one particular realization of the fibre fragmentation with ($\sigma_0 = 1500$ MPa, $m = 9$, $\beta^{-1} = 0.325$ mm). After the first few fibre breaks, the applied stresses must be larger than the actual flaw strengths because of the incomplete stress recovery, expressed by Equation 5a, in the small fragments.

The final cumulative fragment length distributions for the three good fits shown in Fig. 8 are compared to the average experimental data in Fig. 10a–c. Here, the fragments from the six individual tests were combined

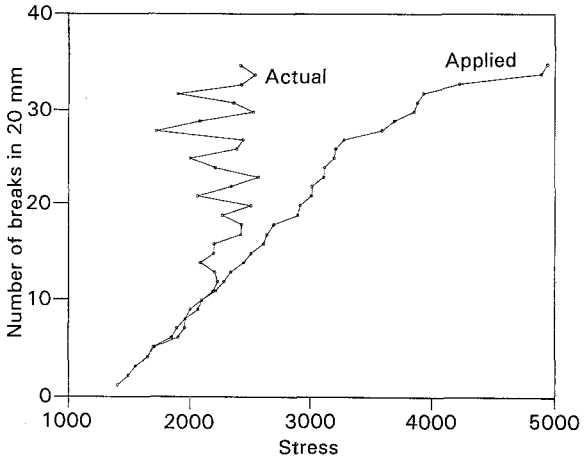

Figure 9 Actual flaw strengths and applied fibre breaking stresses for one typical simulated fibre fragmentation test using the elastic interface model.

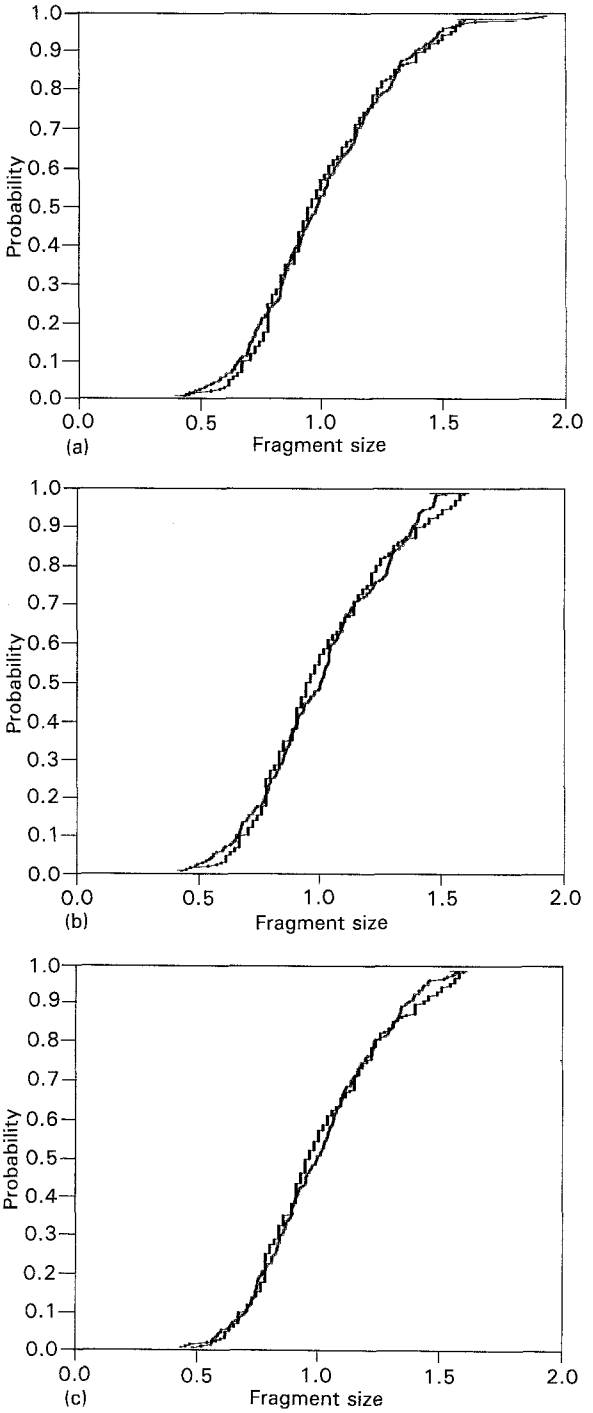

Figure 10 Final cumulative fibre fragment length distributions predicted for elastic shear stress interface model, for good fit values of (σ_0, m, β^{-1}) obtained in Fig. 8; also shown is cumulative data from Fig. 5 (solid symbols). (a) ($\sigma_0 = 1400$ MPa, $m = 7$, $\beta^{-1} = 0.300$ mm); (b) ($\sigma_0 = 1500$ MPa, $m = 9$, $\beta^{-1} = 0.325$ mm); (c) ($\sigma_0 = 1600$ MPa, $m = 11$, $\beta^{-1} = 0.325$ mm).

to form one cumulative distribution. The agreement is quite good for all three cases, particularly for the (σ_0 = 1400 MPa, m = 7, β^{-1} = 0.300 mm) case.

The simulation results for strength versus "instantaneous" fragment length for the three good-fit values of (σ_0, m, β) are compared with the experimental results in Fig. 11a–c. As for Fig. 7, the strengths at the longer fragment lengths (corresponding to the first few breaks) are best fit by the higher Weibull moduli. Linear fits to the simulation data between 2.05 and 20 mm yield apparent Weibull moduli of m* = 4.0, 6.3 and 5.6 for the true values of m = 7, 9 and 11, respectively. The experimental value is m* ~ 6.3; the experimental data agrees best with the (σ_o = 1500 MPa, m = 9, β^{-1} = 0.325 mm) parameter set.

Finally, note that the values of β^{-1} used for all of the good fits obtained in Figs 7, 8 and 10 are in the range of 0.300–0.350 mm. Estimates of β^{-1} from Equation 2c, with d = 35 μm, were β^{-1} = 0.28 for K = 1 and β^{-1} = 0.39 for K = 2. The good agreement in the value of β^{-1} thus gives additional confidence in the appropriateness of the elastic shear stress model to this fibre epoxy system. With the cut-off value of 5 GPa in the applied stress, an estimate for the shear stress at the onset of some sort of inelastic behaviour, such as matrix yielding or debonding, is $\tau_f = \alpha\sigma_0$ = 110–160 MPa. Although such values of τ_f are rather high for this epoxy of macroscopic tensile strength 80 MPa, the precise constraint conditions prevailing in the matrix around the rough, interlocking fibre lead us to interpret the high τ_f as some effective shear strength. In previous studies on carbon fibres, the interfacial shear strengths determined from both s.f.c. tests and pull-out tests are comparable to, but do not directly correlate with, the yield stress of the bulk epoxy.

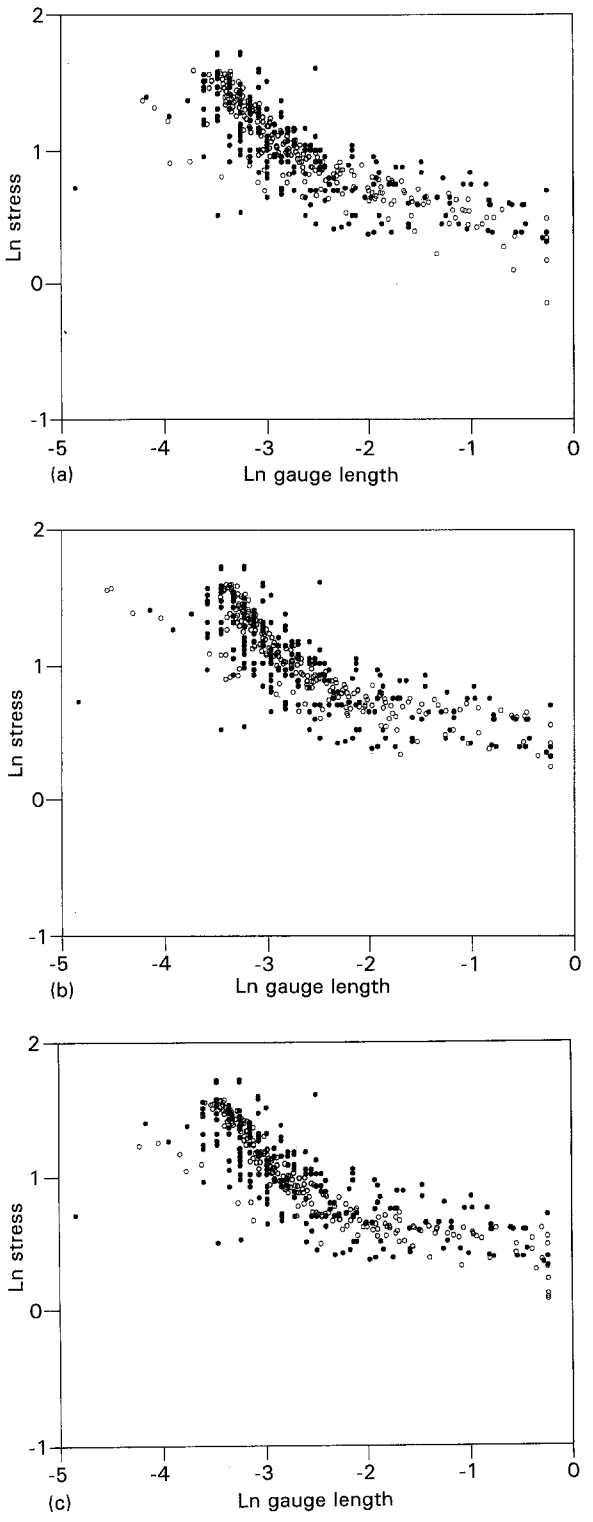

Figure 11 Fibre strength versus fragment size (instantaneous gauge length) as predicated for elastic shear stress interface model, for good fit values of (σ_0, m, β^{-1}) obtained in Fig. 8; also shown is experimental data from Fig. 6 (solid symbols). (a) (σ_0 = 1400 MPa, m = 7, β^{-1} = 0.300 mm); (b) (σ_0 = 1500 MPa, m = 9, β^{-1} = 0.325 mm); (c) (σ_0 = 1500 MPa, m = 11, β^{-1} = 0.350 mm).

5. Discussion

The elastic interfacial shear stress model is clearly capable of accurately describing all of the s.f.c data obtained on the Carborundum SiC fibre/epoxy system studied here. Good fits to the experimental data are obtained over a narrow range of fibre strengths, σ_0 = 1400–1600 MPa at a gauge length L_0 = 20 mm with a Weibull modulus in the range of m = 7–11. The most satisfactory overall agreement is obtained for (σ_0 = 1500 MPa, m = 9), based primarily on the be-

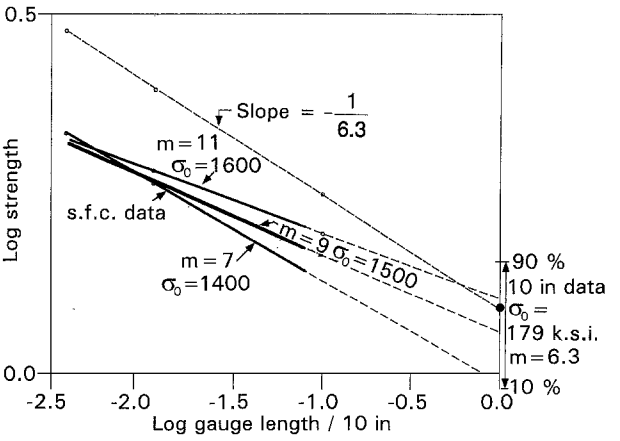

Figure 12 Fibre strength versus gauge length for good-fit strength values derived from the s.f.c. test data; dashed lines show extrapolated strengths at longer gauge lengths. Also shown is the 254 mm single fibre tension test strength and the predicted size dependence (dashed line) based on the estimated Weibull modulus m = 6.3 from the 254 mm tests.

haviour in the early stages of the s.f.c. test where few breaks have occurred. Fig. 12 shows a Weibull plot of strength versus fibre gauge length obtained using the various good-fit values of σ_0 and m in Equation 8. Over the range of small gauge lengths of 1–5 mm probed directly by the fragmentation test, the three pairs of (σ_0, m) values yield very similar results and it is only at the longer gauge lengths of $L > 10$ mm, and in the extrapolation out to even longer gauge lengths, that the predictions of the three differ significantly. Also shown in Fig. 12 is the single-fibre tension test (s.f.t.t.) scale strength, $\sigma_0 = 1225$ MPa, obtained on the Carborundum fibres at a 254 mm gauge length and a fiducial line of extrapolated strength versus gauge length corresponding to the Weibull modulus of m = 6.3 derived from that data [16]. While the good-fit value of ($\sigma_0 = 1400$ MPa, m = 7) gives the closest agreement on the Weibull modulus, the extrapolated strengths at 254 mm are well below the s.f.t.t. scale strength, and this parameter set provides the poorest fit to the s.f.c. data on the low strength range (see Fig. 7). In contrast, the extrapolations for the other two good-fit values bracket the 254 mm strength but give larger m values.

A deviation in Weibull modulus between the value derived from the s.f.c. data at small gauge lengths ($m \sim 9$) and that from the s.f.t.t. data at 254 mm could be attributed to several different factors. First, the flaw population influencing the 254 mm s.f.t.t. data may have included defects which occurred very infrequently in shorter gauge lengths. In fact, the weakest strengths in the 254 mm s.f.t.t. test data have been identified as large pores on the fracture surface, whereas the majority of defects appeared to be grain boundary cracks. Eliminating the population of pore-related failures from the s.f.t.t. test data increases the 254 mm scale strength to 1282 MPa and the Weibull modulus to 7.6 [17]. Secondly, there may have existed fibre-to-fibre variability which tends to give a broader spread (smaller m) to strength distributions than is relevant for describing the flaw populations of each individual fibre. Thus, the s.f.t.t test on 50 254 mm fibre samples (50 total breaks) may have yielded greater variability than the s.f.c. test on five 20 mm samples (212 total breaks). Fibre-to-fibre variability within the five s.f.c. tests alone is reflected in the fact that, although very good fits to the average results can be found for a single (σ_0, m) value, the variability in the experimental data (Fig. 4, for instance) was greater than the variability found in the simulation results. Some of the variability may have been due to errors in the calibration of sample strain with fibre stress, the thermal stress correction, or variations in the interfacial β-value, but the variability may also reflect some small intrinsic fibre-to-fibre variability which has yet to be identified. Such variability may also exist in other types of fibres which, however, have yet to be subject to the extreme scrutiny afforded by the s.f.c. tests.

The strength behaviour at the small gauge lengths relevant in composites is now discussed. The tensile strength of a ceramic matrix composite depends on the fibre strength at the length δ_c given by [18]:

$$\delta_c = \left[\frac{\sigma_0 d L_0^{1/m}}{2\tau}\right]^{m/m+1} \quad (14)$$

where τ is the sliding resistance between the fibre and matrix. For certain coatings on these types of SiC fibres, a value of $\tau = 8$ MPa has been derived from fibre push-out experiments [19]. Utilizing the three good-fit values of (σ_0, m) obtained here and $d = 35$ μm gives:

$$\delta_c = 3.9 \text{ mm} \quad (15)$$

as the relevant gauge length and corresponding strength of

$$\sigma_c \sim 1750 \text{ MPa} \quad (16)$$

nearly independent of which good-fit values of (σ_0, m) were used.

The theoretical ultimate tensile strength, σ_u, of a CMC composite made with these coated fibres was then $\sigma_u = f\phi(m)\sigma_c$, where $\phi(m) = 0.74$–0.79 for m = 7–11, respectively [18]. Thus, using Equation 16 the predicted composite strength is

$$\sigma_u = f(1340 \pm 50) \text{ MPa} \quad (17)$$

for a volume fraction f of fibres aligned in the tensile direction. These strength values are comparable to the strengths obtained from other ceramic matrix composites with fine diameter SiC-based fibres, such as Nicalon [20]. Thus, the present strength level for the Carborundum SiC fibres is sufficient for good composite behaviour assuming no degradation of the fibre strength properties upon composite processing.

Finally, it is again emphasized that close attention to the fibre/matrix interface behaviour is necessary for properly interpreting the s.f.c. data and determining the fibre strength distribution. For instance, using the constant shear stress model gives fair agreement, on cursory analysis, with ($\sigma_0 = 1000$ MPa, m = 3). However, extrapolating to other gauge lengths leads to a large overestimation of the fibre strength at small lengths ($\sigma = 2700$ MPa at 1 mm) and a large underestimate of the strength at long gauge lengths ($\sigma = 429$ MPa at 254 mm). Of course, the shear lag model used here to describe the elastic interface may have its limitations and further development of the model would be desirable for future analyses. But, the model is probably sufficiently good (especially with β as a free parameter) for use as a distinct alternative to the constant shear model often assumed a priori. In any case, the present work demonstrates that, with careful testing and simultaneous analysis of a variety of largely independent aspects of the s.f.c. data, a good consistent understanding of the entire fibre fragmentation process can be obtained. The s.f.c. technique can therefore be an accurate and efficient method for obtaining fibre strength distributions, particularly at small gauge lengths.

References

1. A. G. METCALFE and G. K. SCHMITZ, in Proceedings of the 67th Meeting of the ASTM (ASTM, Philadelphia, PA, 1964) p. 1075.

2. A. KELLY and W. R. TYSON, *J. Mech. Phys. Solids* **13** (1965) 329.
3. B. W. ROSEN, *AIAA J.* **2** (1964) 1985; C. Zweben and B. W. Rosen, *AIAA J.* **6** (1968) 2325.
4. W. A. FRASER, F. H. ANCKER, A. T. DIBENEDETTO and B. ELBIRLI, *Polym. Comp.* **4** (1983) 238.
5. L. T. DRZAL, M. J. RICH and P. F. LLOYD, *J. Adhesion* **16** (1982) 1.
6. S. H. OWN, R. V. SUBRAMANIAN and S. C. SAUNDERS, *J. Mater. Sci.* **21** (1986) 3912.
7. W. D. BASCOM and R. M. JENSEN, *J. Adhesion* **19** (1986) 219.
8. A. N. NETRAVALI, R. B. HENSTENBURG, S. L. PHOENIX and P. SCHWARTZ, *Polym. Comp.* **10** (1989) 226.
9. B. YAVIN, H. E. GALLIS, J. SCHERF, A. EITAN and H. D. WAGNER, *Polym. Comp.* **12** (1991) 436.
10. H. L. COX, *Brit. J. Appl. Phys.* **3** (1951) 72.
11. W. A. CURTIN, *J. Mater. Sci.* **26** (1991) 5239.
12. W. WEIBULL, *J. Appl. Mech. (ASME)* **18** (1951) 293.
13. R. B. HENSTENBURG and S. L. PHOENIX, *Polym. Comp.* **10** (1989) 385.
14. A. KELLY and N. H. MACMILLAN, "Strong solids", 3rd Edn (Clarendon Press, Oxford, 1986) Ch. 6.
15. W. A. CURTIN, accepted in *Polym. Comp.*
16. G. V. SRINIVASAN and V. VENKATESWARAN, in Proceedings of the 17th Annual Conference on Composites and Ceramics, Cocoa Beach, FL (1993)
17. G. V. SRINIVASAN, Private communication.
18. W. A. CURTIN, *J. Amer. Ceram. Soc.* **74** (1991) 2837.
19. W. A. CURTIN, J. I. ELDRIDGE and G. V. SRINIVASAN, *J. Am. Cer. Soc.* **76** (1993) 2300.
20. H. C. CAO, E. BISCHOFF, O. SBAIZERO, M. RUHLE, A. G. EVANS, D. B. MARSHALL and J. J. BRENNAN, *J. Amer. Ceram. Soc.* **73** (1989) 1691.

Received 2 August 1993
and accepted 28 February 1994